Modification of Edge Profiles, Edge Transport, and ELM Stability with Lithium in NSTX

R. Maingi[1], D. Boyle[2], J.M. Canik[1], J. Manickam[3], T.H. Osborne[4], P.B. Snyder[4], R.E. Bell[3], S.P. Gerhardt[3], R. Kaita[3], H.W. Kugel[3], B.P. LeBlanc[3], D.K. Mansfield[3], S.A. Sabbagh[5], and the NSTX team

Email: rmaingi@pppl.gov
[1] *Oak Ridge National Laboratory, PO Box 2008, Oak Ridge TN, 37831 USA*
[2] *Princeton University, Princeton, NJ, 08543 USA*
[3] *Princeton Plasma Physics Laboratory, Princeton, NJ, 08543 USA*
[4] *General Atomics, San Diego, CA 92121 USA*
[5] *Columbia University, New York, NY 10027 USA*

Abstract. We report results of an experiment in which lithium wall coatings were gradually introduced into NSTX, resulting in a gradual improvement in energy confinement, alteration of edge plasma profiles, and growing periods of ELM suppression. As a result of increasing lithium wall coatings, recycling and edge fueling were reduced, which relaxed the edge density profile gradients. In contrast, the edge T_e profile was unaffected in the H-mode pedestal steep gradient region at constant plasma stored energy; however, the region of steep T_e gradients extended radially inward by several cm following lithium coatings. Consequently, the pressure profile width and pedestal height increased substantially, while the ELM-free discharge peak pressure gradients were comparable to the pre-lithium ELMy discharge gradients. The measured edge profiles in discharges with and without lithium were simulated with the SOLPS code, which indicated that both a reduction in recycling *and* a drop in the edge and SOL cross-field transport was required to match the post-lithium profiles. Edge stability calculations showed that the discharges with lithium coatings were farther from the low-n kink/peeling modes boundary than the pre-lithium discharges.

I. Introduction

Rapidly growing instabilities known as Edge Localized Modes (ELMs) are commonly observed in high-confinement (H-mode) regimes in many toroidal confinement devices. The reduction or elimination of ELMs with high confinement is essential for the ITER, which has been designed for H-mode operation. Detailed analysis has shown that large ELMs are triggered by exceeding either edge current density limits (kink/peeling modes) and/or edge pressure gradient limits (ballooning modes)[1-3]. Similar edge stability calculations using model equilibria have indicated that spherical tokamaks should have access to higher pressure gradients and H-mode pedestal heights than higher aspect ratio tokamaks, owing to high magnetic shear and possible access to second stability regimes[4]. However spherical tokamaks have observed a wide variety of ELM types, many in common with higher aspect ratio tokamaks[5, 6]; true ELM-free regimes with high pedestal pressure gradients have been rare. The use of lithium in NSTX has enabled access to such a high pedestal pressure regime, one in which the core stability limits with high normalized beta are observed with no sign of ELMs[7].

II. Description of Experiment: Sequence from ELMy to ELM-free discharges

Lithium wall coatings were introduced into NSTX in 2005 as a wall conditioning and confinement improvement tool[8]. The confinement improvement was shown to occur mainly in the electron transport channel[9], with the magnitude of the improvement depending on the

amount of lithium deposited between discharges[10]. Separately it was observed that lithium wall coatings seemed to suppress ELMs for sufficiently lithium high evaporation rates[11].

A scenario with ordinary Type I ELMs was observed several years ago in an Alcator C-Mod/MAST/NSTX similarity experiment[12] on small ELM regimes. These ELMs had a fractional stored energy drop $\Delta W/W \sim 2\text{-}5\%$, nominal frequency of ~ 100 Hz that increased with heating power, in a boundary shape with a relatively high X-point for NSTX, with $\delta_r^{sep} \sim -5$mm. Here δ_r^{sep} is the distance between the two X-points mapped to the outer midplane, where the convention $\delta_r^{sep} < 0$ means the lower X-point is closer to the plasma.

An experiment was conducted in which lithium coatings were systematically introduced into the ELMy discharges described above, with a pair of overhead evaporators at constant evaporation between discharges, to investigate the mechanism by which ELMs were suppressed[13]. This sequence was the first use of lithium in this campaign, insuring that the reference discharges were truly pre-lithium. Relevant discharge parameters were: plasma current I_p=0.8 MA, vacuum toroidal field B_t=0.45 T, and neutral beam injected power P_{NBI}=4 MW. The gas fueling, P_{NBI}, and shape were held constant until the very end of the scan, when higher fueling and lower P_{NBI} were needed to avoid low density locked modes and resistive wall modes. It was shown that the ELMs were suppressed during phases of quiescence, whose duration increased gradually. The growth of these quiescent phases was not monotonic, however; discharges that had rotating tearing modes that slowed down and locked were followed by increased ELM activity in the subsequent discharge.

In the remainder of this paper, we will first compare the reference ELMy discharges and the final ELM-free discharges with reduced P_{NBI}. We will subsequently present profile analysis for many discharges during the sequence, showing that the observed ELM frequency variability correlate with the broadening of the density and pressure profiles.

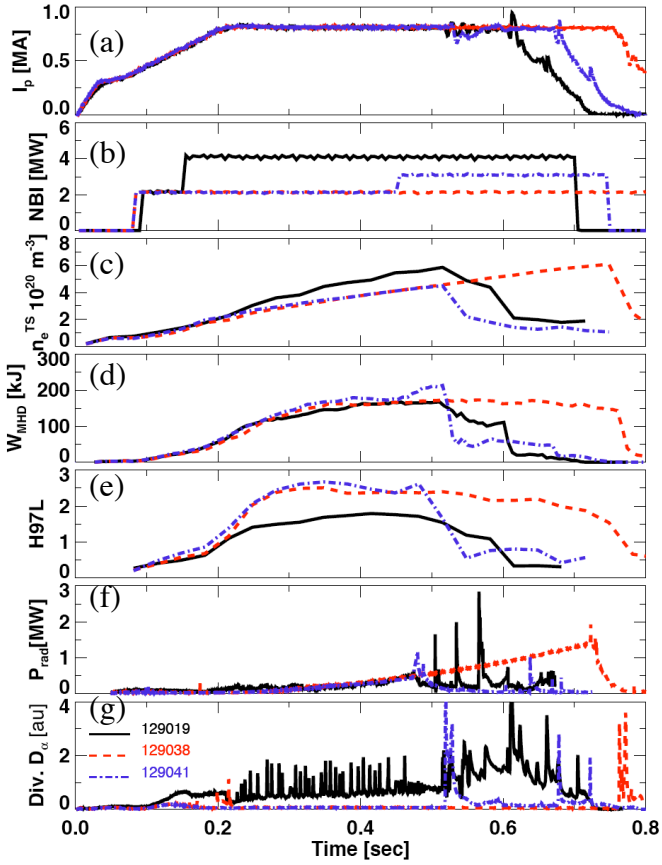

Fig. 1. Comparison of pre-lithium ELMy discharge (black), and two discharges with lithium at different NBI power (blue, red): (a) plasma current I_p, (b) neutral beam injected power P_{NBI}, (c) line-average density from Thomson Scattering n_e^{TS}, (d) stored energy from equilibrium reconstruction W_{MHD}, (e) confinement time relative to ITER97L scaling, (f) total radiated power P_{rad}, and (g) divertor D_α emission.

IIa. Transport and Stability at End points of Sequence

With a high lithium evaporation rate (≥ 15 mg/min) and/or coating thickness (≥ 1 g), the energy confinement τ_E increased such that the heating power needed to be reduced to avoid the global stability limit at the end point of the discharge sequence[7, 13]. The effect of thick lithium wall coatings on discharge characteristics is shown for three

discharges (black: pre-lithium ELMy, red: with lithium, low power, blue: with lithium, intermediate power) in Fig. 1. The red and blue discharges occurred at the end of the discharge sequence discussed in II. Panel 1b shows a step in P_{NBI} from 2 to 3 MW at 0.45 sec in the discharges with lithium. Note that the discharges with lithium near the end of the sequence with P_{NBI}=4 MW disrupted shortly after the I_p flat-top (not shown). The discharges with lithium in Fig. 1 showed reduced early density and dN/dt, although the eventual density in the lowest power discharge reached the same value as the reference discharge, partly because of the lack of ELMs (panel 1c). Panel 1d shows that the stored energy for the 2-MW discharge was comparable to the 4-MW ELMy discharge, and that the τ_E normalized by the ITER-97 L-mode global scaling[14] was 50% higher in the with-lithium discharges (panel 1e). Following the 2 MW-3 MW step at 0.45 sec, a global MHD instability with signatures of a resistive wall mode terminated the high performance phase (blue curve panel 1d). The radiated power was comparable out to 0.48 sec in these discharges, despite higher input in the ELMy discharge, i.e. the radiated power fraction increased during the ELM-free H-mode phase (panel 1f). Finally the divertor D_α emission was substantially lower in the with-lithium discharges, indicating reduced recycling, and ELM activity completely vanished (panel 1g).

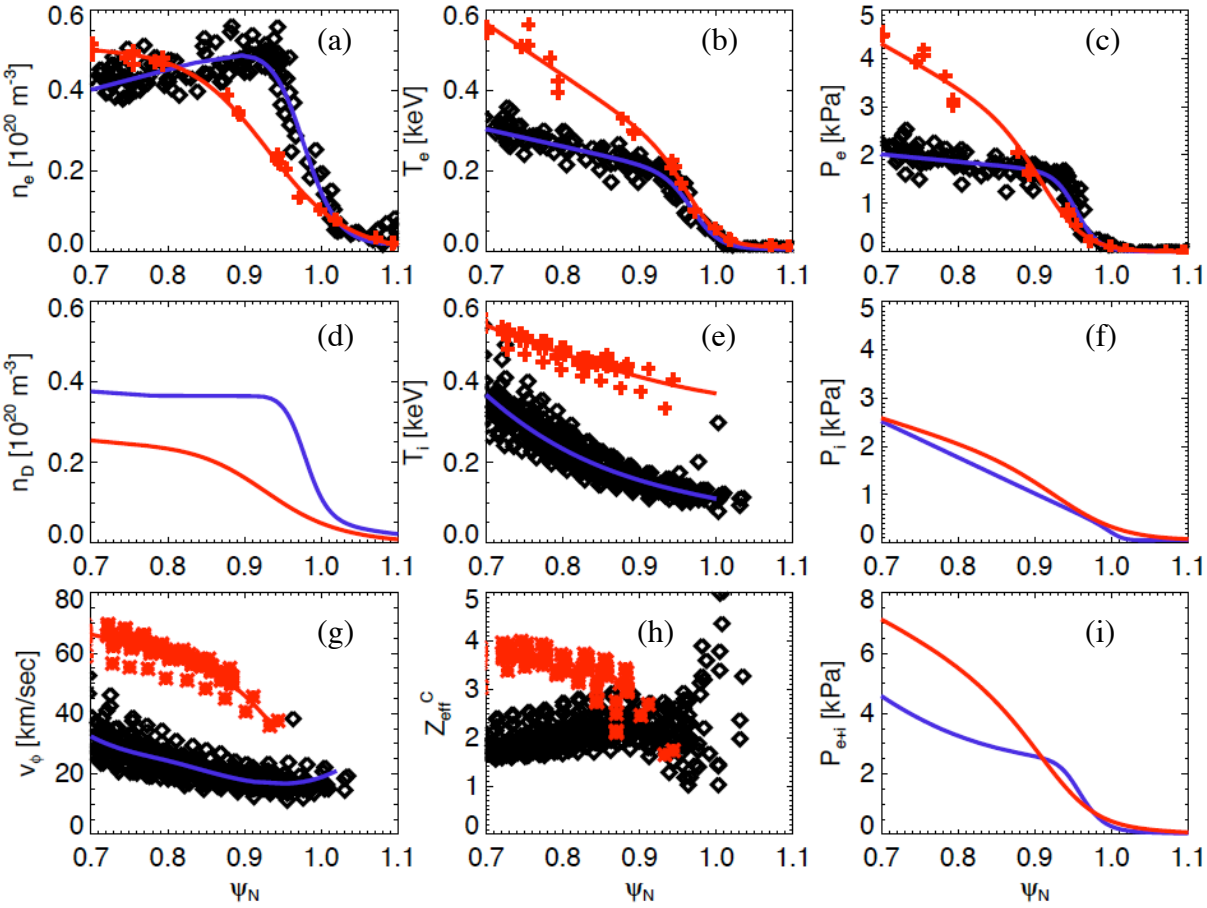

Fig. 2. Profile comparisons from initial ELMy discharge without lithium (black data, blue curve fits) and near-final ELM-free one with lithium (red data/fits). Fits are obtained from multiple time slices mapped to the nearest equilibrium. The x-axis is normalized poloidal flux: $\psi_N = (\psi_o-\psi)/(\psi_o-\psi_{sep})$, where ψ_o and ψ_{sep} are the poloidal flux values at the magnetic axis and separatrix, respectively.

The dramatic effect of lithium conditioning on the plasma kinetic profiles for the 2 MW with-lithium and 4 MW pre-lithium discharges from Figure 1 is displayed in Fig. 2. The technique used for the profile analysis is described elsewhere[15]. The electron density n_e gradient was

clearly reduced, the electron temperature T_e gradient was comparable from ψ_N to 0.95-1.0, but the steep gradient region merely extended into ψ_N of 0.8 in the with-lithium discharge. Consequently the peak electron pressure P_e gradient was shifted radially inward farther from the separatrix, and the pressure profile width increased. The with-lithium discharge also had a reduced deuteron density gradient, a higher edge ion temperature, but a comparable edge ion pressure gradient. The total pressure gradient was dominated by the electron gradients in both cases. The with-lithium discharge also had higher edge rotation speed v_ϕ, and also higher carbon density and resulting Z_{eff} (from carbon), the latter because of the reduced impurity confinement in the ELMy pre-lithium discharge.

The two sets of edge profiles in Figure 2 were simulated[16] with the 2-D edge plasma and neutrals code SOLPS[17], to quantify the change in edge recycling and transport. These calculations were also constrained by divertor heat flux profiles (for power balance), divertor D_α profiles (for divertor recycling coefficient R_p). Fig. 3 shows that the edge transport coefficients for both particles (D) and electron energy (χ_e) in the ELMy discharge had a minimum in the region of the steep gradient region from $0.94<\psi_N<1$, indicative of the transport barrier. In contrast, the discharge with lithium had reduced transport rates inside of this region, i.e. from $0.8<\psi_N<0.94$, down to the H-mode levels in the steep gradient region. Effectively the region of low transport extended to the inner boundary of the calculation, $\psi_N=0.8$. On the other hand, the transport in the steep gradient region was unchanged, indicating a resilient mechanism that prevented the T_e gradients from increasing further with reduced density gradient, e.g. electron temperature gradient (ETG) modes. For reference, the R_p was reduced from 0.98 to 0.92 in the discharge with lithium[16]. We note that no attempt was made to separate diffusive transport and pinch terms, i.e. the inferred diffusivity is an 'effective D' only.

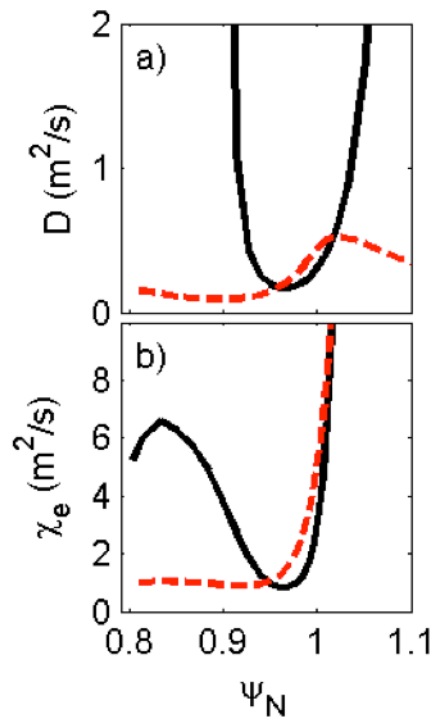

Fig. 3 – Comparison of computed a) particle and b) electron thermal diffusivity for pre-li (solid black - #129015) and with-li (dashed red - #129038) discharges.

A comparison of the plasma total pressure profile and its radial gradient from representative free boundary kinetic eqilibria[7] the were constrained by the profiles in Fig. 2 for the reference and with-lithium discharges is shown in Figure 4. Note that the profiles were obtained from five reference ELMy discharges to maximize the number of profiles in the last 20% of the ELM cycle. The pre-lithium discharge had a steep pressure gradient very near the separatrix (ψ_N =1), whereas the peak gradient was shifted inward substantially for the with-lithium time slices (Fig. 4a, 4b), owing primarily to the reduction of the density gradient. Fig. 4b also shows that the peak pressure gradient can actually be higher in the with-lithium discharges, i.e. the reason for enhanced stability is not simply a reduction in the peak pressure gradient. In addition the spatial width of the steep gradient region is larger in the post-lithium discharge, i.e. from $0.8<\psi_N<1$.

Calculations with the PEST[18] and ELITE codes[2, 3] both showed[7] that the with-lithium discharges were farther from their stability boundaries than the reference pre-lithium ELMy

discharges. Fig. 4c shows that the ELMy discharge was relatively close to the kink/peeling side of the boundary. The low aspect ratio naturally results in the ballooning instability being at much higher normalized pressure gradients, i.e. far to the right of the shown diagrams. Fig. 4d shows that the separation between the experimental equilibrium and its stability boundary increased substantially. The two reasons for the movement of the stability boundary are: 1) the peak pressure gradient and calculated edge bootstrap current peak were shifted inboard farther from the separatrix, which is stabilizing for the peeling mode drive, and 2) the pedestal width and height increased substantially, which is also stabilizing.

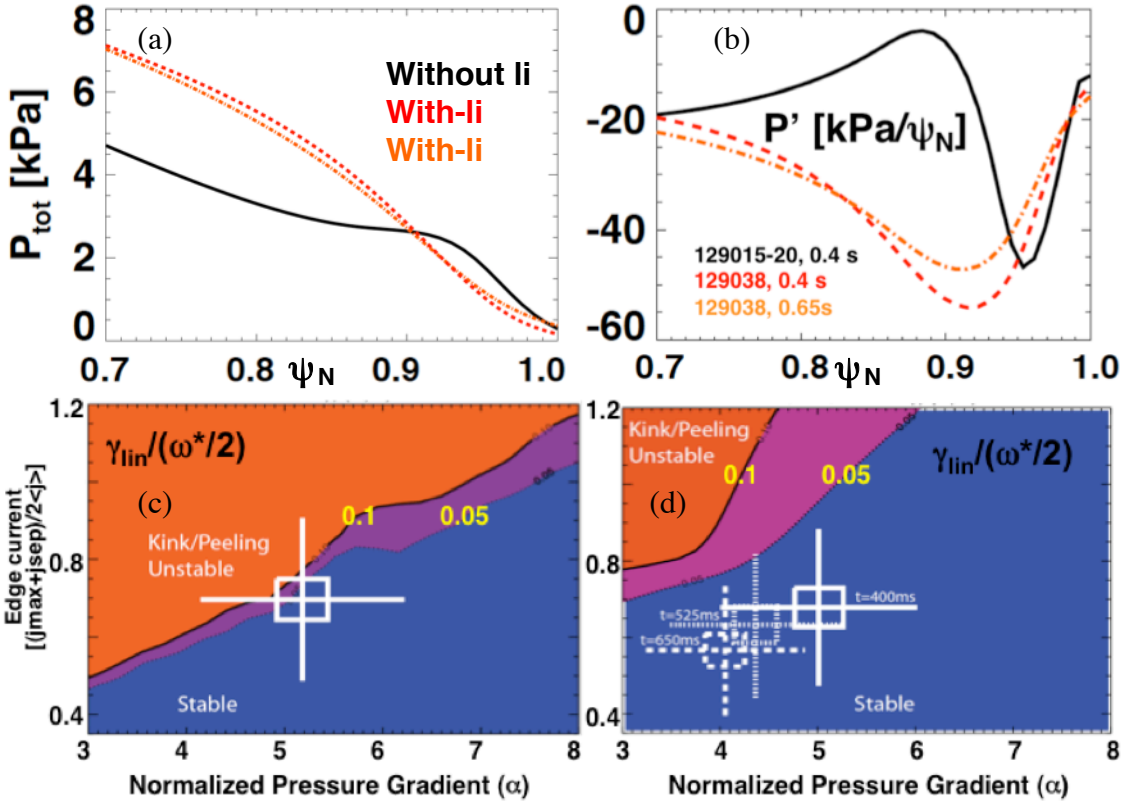

Fig. 4 – (a) Kinetic pressure and (b) pressure gradient in normalized flux space for the pre- and post-lithium equilibria; stability boundary (blue to orange color transition) from ELITE code with fixed boundary kinetic EFITs for (c) pre-lithium discharge and (d) discharge with lithium coatings.

IIb. Profile evolution during Discharge Sequence

As mentioned in II and illustrated in Fig. 5, the discharges did not simply change from ELMy to ELM-free (although this has been accomplished with large amounts of lithium evaporated between discharges). Lithium was added following #129019. Fig. 6a shows the measured ELM frequency during discharges from this sequence (discharge 1 is #129015). The data points in black had edge profiles that could be analyzed as described above. There are several discharges with more than one data point per discharge; in those cases, the edge profiles were analyzed in non-overlapping time windows of duration ~ 0.1 sec. The first six discharges were all reference ELMy pre-lithium discharges, and lithium was introduced after discharge #6. Discharges 7-10 showed a small but measurable decrease in ELM frequency, whereas discharge 11 had an ELMy phase and a long ELM-free phase. Discharge 13 was ELMy again and followed an ohmic discharge, which we conjecture changed the edge recycling as compared with the NBI heated discharges. Note that discharge #16 had both an ELMy and an ELM-free window. Discharge 17 again had a long ELM-free phase, but it had a tearing mode that locked; the subsequent discharge #18 was ELMy again. Finally discharges 19-23 had

high beta locked modes, and discharge #24 (#129038 in Fig.1) had reduced NBI power, higher fueling, and was completely ELM-free. Discharge #27 (#129041) was used to assess the β_N limit, as shown in Fig. 1.

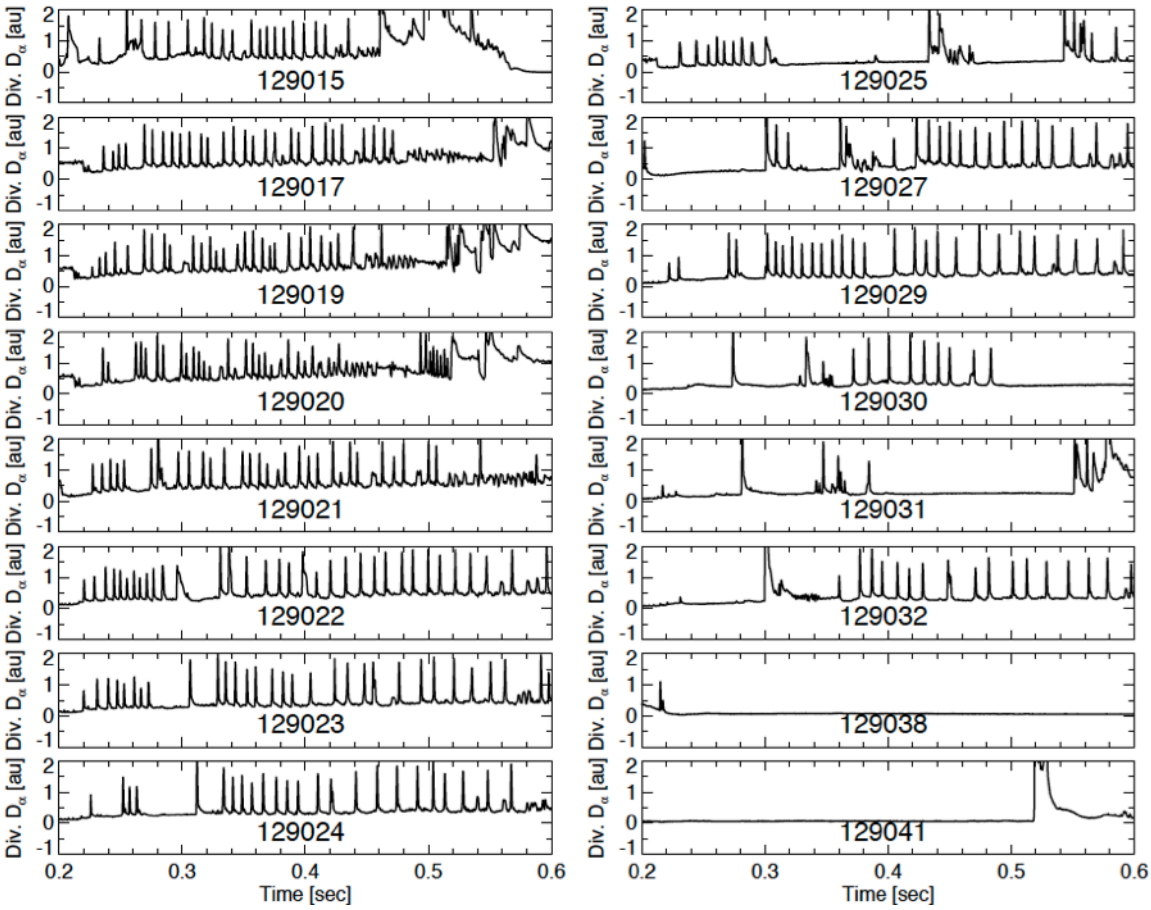

Fig. 5 – ELM activity vs. discharge number in experiment

The n_e, T_e, and P_e profiles were fitted with a 'standard' modified tanh function[19], which includes both a tanh component and a linear component; these pedestal widths, along with the top of the P_e pedestal, are shown in Figs. 6c-f. The width of the total pressure gradient (full-width half-max) is shown in Fig. 6b; this latter width is bigger than the mtanh pedestal pressure widths because the ion pressure profile is broader than the electron, and because of the functional form of the fit. The T_e profile width can be immediately ruled out as an ordering parameter. The n_e profile width, pressure gradient width, and P_e pedestal height are all shown to order the ELMy and ELM-free data, mostly as a threshold criterion. The evidence for a gradual relation between ELM frequency and widths is being assessed. Since the lithium mainly changes the recycling and the edge fueling, these trends support the hypothesis that the density profile gradient reduction is the controlling physics.

III. Summary, Conclusions, and Acknowledgements

To summarize, lithium wall coatings suppressed ELMs in otherwise Type I ELMy NSTX discharges, owing ostensibly to reduction in both recycling and core fueling. The plasma profiles changed substantially as a result, with a reduction in the n_e profile gradient, which caused an inward shift of the pressure profile gradient since the edge T_e gradient remained ~ constant in the H-mode barrier region.

Interpretive simulations with the SOLPS code showed that the edge D and χ_e were reduced substantially from 0.8-ψ_N-0.94, i.e. the H-mode pedestal effectively expanded to the inner boundary of the calculation in the ELM-free discharge with lithium. On the other hand, the D and χ_e were largely unchanged from 0.95-1, suggesting an instability that limits the gradient in that region. The inferred transport reduction can be partly accounted because the lithium discharge had only 1/2 the P_{NBI} of the reference discharge, and should have somewhat lower transport in light of the well-known confinement degradation with P_{NBI}. Present research in this area is focused on correlated and quantifying these reduced transport rates with a measured reduction in edge turbulence.

Ultimately, the reduction in the density profile gradient shifted the steep pressure gradient farther from the separatrix, which helped to stabilize the kink/peeling instabilities. The broadening of the pressure profile was also stabilizing. Specifically the pre-lithium (with-lithium) profiles were unstable (stable) to low-n=2-4 peeling/ballooning modes, based on calculations from the PEST and ELITE codes. That these were actually low-n instabilities is supported by observations of pre-cursor oscillations in the fast magnetics data, which were present in the pre-lithium discharges and absent in with-lithium discharges. We note there are uncertainties in our analysis procedure, particularly due to the lack of an edge current measurement, and hence there is a need to test other theories of ELM suppression[20].

The discharges enabled by the lithium conditioning become ELM-free with a substantial improvement in energy confinement time relative to scalings. Consequently the discharges

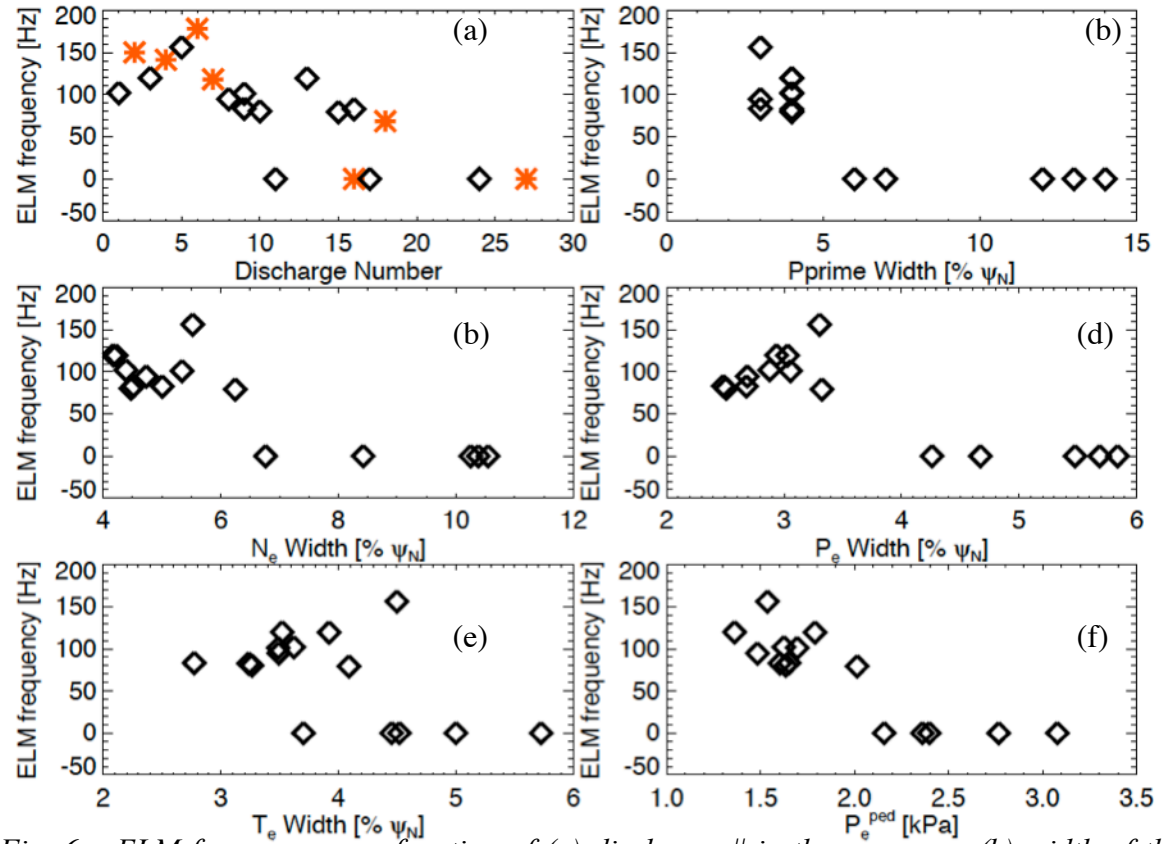

Fig. 6 – ELM frequency as a function of (a) discharge # in the sequence, (b) width of the pressure gradient, (c) n_e profile width, (d) P_e profile width, (e) T_e profile width, and (f) P_e pedestal height. Panels (c)-(f) are obtained from the modified tanh fitting function, and panel (b) is defined in the text. The red data points in panel (a) are from discharges in the sequence whose profile data could not be fitted with the standard procedure.

achieved normalized beta β_N of 5.5, where $\beta_N = aB_t\beta/I_p$, a = minor radius, β = ratio of average plasma pressure to toroidal magnetic field pressure ($B_t^2/2\mu_0$), and μ_0 = permeability of free space. The global instability that terminated the high performance phase in Figure 1 had characteristic signatures of a resistive wall mode, indicating that the discharge was operating between the 'no-wall' and 'ideal-wall' β limits in NSTX[21]. In other words, the lithium-enhanced discharges reached global stability limits before reaching edge/ELM stability limits, thereby avoiding large pulsed power loads to the target. Looking ahead, quantitative understanding of the effect of the lithium wall coatings on the density profile remains an area of active research for projection of the effects of lithium in other devices, and research on optimization of triggered ELM scenarios to flush impurities is continuing[22-25].

One outstanding question is the role of diamagnetic stabilization in NSTX. The kink/peeling mode linear growth rates γ_{lin} in NSTX are computed to be ~ 1% of the Alfven frequency ω_A, which should be stabilized by the diamagnetic drift, ω_*. Indeed the value of $\gamma_{lin}/(\omega_*/2)$ at the onset of the instabilities in NSTX is 0.05-0.1 as shown in Fig. 4c, i.e. ~ 1/10 of the value from DIII-D and other devices[2, 4]. Near term research is focused on improving the diamagnetic stabilization calculation at low aspect ratio, as well as improving the spatial resolution of the Thomson Scattering measurements to better resolve the edge gradients.

This research was supported in part by the U.S. Deptartment of Energy under contracts DE-AC05-00OR22725, DE-AC02-09CH11466, DE-FC02-04ER54698, DE-AC52-07NA27344, DE-FG03-99ER54527 and DE-FG02-99ER54524. We gratefully acknowledge the contribution of the NSTX technical and operations staff, and acknowledge a prediction of ELM suppression with lithium by L.E. Zakharov in advance of the experiment.

References

1 J. W. Connor, *et al*., *Phys. Plasma* **5** (1998) 2687.
2 P. B. Snyder, *et al*., *Phys. Plasma* **9** (2002) 2037.
3 H. R. Wilson, *et al*., *Phys. Plasma* **9** (2002) 1277.
4 P. B. Snyder, *et al*., *Plasma Phys. Contr. Fusion* **46** (2004) A131.
5 R. Maingi, *et al*., *Nucl. Fusion* **45** (2005) 1066.
6 A. Kirk, *et al*., *Plasma Phys. Contr. Fusion* **46** (2003) 551.
7 R. Maingi, *et al*., *Phys. Rev. Lett.* **103** (2009) 075001.
8 H. W. Kugel, *et al*., *Plasma Phys. Contr. Fusion* **51** (2009) 124054.
10 S. Ding, *et al*., *Plasma Phys. Contr. Fusion* **52** (2010) 015001.
11 H. W. Kugel, *et al*., *Phys. Plasma* **15** (2008) 056118.
12 R. Maingi, *et al*., *Nucl. Fusion* (2010) submitted.
13 D. K. Mansfield, *et al*., *J. Nucl. Materials* **390-391** (2009) 764.
14 S. M. Kaye, *et al*., *Nucl. Fusion* **37** (1997) 1303.
15 T. H. Osborne, *et al*., *J. Phys.: Conf. Series* **123** (2008) 012014.
16 J. M. Canik, *et al*., *J. Nucl. Mater.* (2010) at press.
17 R. Schneider, *et al*., *Contrib. Plasma Physics* **46** (2006) 3.
18 R. Grimm, *et al*., *Methods Comput. Phys.* **16** (1976) 253.
19 R. J. Groebner, *et al*., *Plasma Phys. Contr. Fusion* **40** (1998) 673.
20 L. E. Zakharov, *et al*., *J. Nucl. Mater.* **363-365** (2007) 453.
21 S. A. Sabbagh, *et al*., *Phys. Plasma* **9** (2002) 2085.
22 J. M. Canik, *et al*., *Phys. Rev. Lett.* **104** (2010) 045001.
23 J. M. Canik, *et al*., *Nucl. Fusion* **50** (2010) 064016.
24 J. M. Canik, *et al*., *Nucl. Fusion* **50** (2010) 034012.
25 J. M. Canik, *et al*., this conference, paper EXC/8-1.